SOURCE POSITION OBSERVABILITY IN A MULTIPATH CHANNEL

M. João Rendas

CAPS, Instituto Superior Técnico
Av. Rovisco Pais, 1096 Lisboa Codex, Portugal

José M. F. Moura*

LASIP, Carnegie Mellon University
Pittsburgh, 15213 PA, USA.

Abstract— This paper studies the impact of the multipath structure of the underwater acoustic channel on the observability of the position of a distant source. Using a recently proposed definition of ambiguity function we study the observability of source position in multipath channels using a propagation model of moderate complexity. To assess the importance of multipath modeling on the observability structure, we compare the ambiguity surfaces to those obtained with propagation models that consider only the spatial structure (wavefront curvature and orientation) of the received wavefield.

1. Introduction

Source localization is an active area of research, finding application in many different fields, either civil (e.g., monitoring of autonomous underwater vehicles) or military (e.g., surveillance and guidance systems). The nature of the medium where the source is, as well as the characteristics of the radiated signal, are key factors that determine the quality of the estimates. Other important factors are the properties of the observing operator (geometry and size of the receiving antenna), and the availability of knowledge about the signal emitted by the source [3].

Simple observer geometries, together with simplistic propagation models (such as line arrays and straight path propagation) impose limitations on the ambiguity structure of the localization problem. Existing ambiguities can be eliminated either by using a more powerful observation operator (array), or by a more accurate modeling of the complex propagation structure of the ocean. Hence, localization systems have evolved towards the use of larger and more complex antennas (e.g., use of twin-line arrays, circular arrays), and of propagation models of increasing complexity (matched field approach). The latter approach has the advantage of not imposing too stringent requirements on the size and shape of the receiving aperture, which may be impractical in many applications. Due to the high complexity of the propagation models, the obervability properties of matched field techniques are difficult to analyze, very few results existing that clearly display its advantages and limitations. This paper is a contribution to this study, discussing the observability of source position using a propagation model of moderate complexity.

One of the key characteristics of underwater sound propagation is the existence of multiple paths between source and receiver, due either to the reflections of sound in the medium's boundaries, or to its continuous refraction. This feature is present in our propagation model [1], which approximates the velocity profile characteristic of large deep ocean areas by a bilinear function of depth. In keeping within the simple framework of ray acoustics, we are able to have insight into the effect of the propagation geometry on global observability, using familiar concepts such as rays, arrival angles, inter-path delays, relative path attenuations, etc..

Source location is an inverse problem: given the noise corrupted version of the output of a propagation operator with known parametric dependency on the source position, infer its true value. In *active* systems, the input to the propagation operator is known, while in *passive* systems, the signal is unknown to the location mechanism. Adequate tools for analyzing the global observability characteristics (ambiguity structure) of active location systems have been proposed decades ago [6], being extensively used by radar and sonar engineers. However, only recently has a general ambiguity definition been advanced [2, 5, 4] which is suitable for either passive or active systems and arbitrary signal bandwidths (narrowband or wideband). In this paper, we use this definition of ambiguity function to study the observability of source position in multipath channels.

We consider the location of a distant wideband source of unknown spectrum by a linear uniform array. The paper presents analytical expressions of the ambiguity surface. For several source/receiver configurations, we show plots that illustrate the distinct behaviors corresponding to shadow and convergence zones, as well as the influence

[1] The work of the second author was partially supported by Darpa through ONR grant N00014-91-J-1833

0-7803-0838-7/92 $3.00

of source spectrum and array geometry.

To assess the importance of multipath modeling on the observability structure, the results are compared to the ambiguity surfaces that describe the source observability for a propagation model that considers only the spatial variation (wavefront curvature and orientation) of the received wavefield. This comparison reveals the advantages in terms of global observability of the complete spatial/temporal modeling of the sensors output.

The paper is organized as follows: In section 2 we present the analytical expressions for the ambiguity surfaces. We consider time/space models, as well as models that capture only the spatial variation of the observed wavefield. The other sections present ambiguity surfaces that result when a bilinear velocity profile is considered (for details on the propagation model, see [1]): In section 3 the overall structure is presented, showing that ambiguity between distinct zones can be present for certain geometries. The next three sections discuss the local (inside each zone) ambiguity structure, for the near Zone (Section 4), the first Shadow Zone (Section 5), and the first Convergence Zone (Section 6).

2. Ambiguity Function

Consider that the observations' power spectrum is described by

$$R_\theta(\omega) = \mathcal{S}(\omega) h_\theta(\omega) h_\theta(\omega)^H + \sigma^2(\omega) I_K$$

where we assume that the observation noise is spatially incoherent, with known power density $\sigma^2(\omega)$. In the previous equation, $\mathcal{S}(\omega)$ is the *unknown* source spectral density and $h_\theta(\omega)$ is the resultant vector, that describes the coherent combination of the steering vectors corresponding to the P replicas received.

The resultant vector can be decomposed as

$$h_\theta(\omega) = D(\theta) b(\theta)$$

where the $K \times P$ matrix $D(\theta)$ describes the spatial structure of the individual replicas, depending only on the inter-sensor delays for each received path, and $b(\theta)$ is a P dimensional vector that depends only on their temporal alignment.

A. Complete Model

When a complete model of the channel is used, the resultant vector is perfectly known for each θ, i.e., both the matrix $D(\theta)$ and the vector $b(\theta)$ in the previous equation are known functions of the source location θ.

In this case, application of the definition of ambiguity introduced in [2, 5] yields the following expression for the ambiguity between scanning location θ, and a source at the true location θ_0 radiating a signal with spectrum $S_0(\omega)$, see [5]:

$$\mathcal{A}(\theta_0,\theta)^{spa/tim}_{S_0} = \int \frac{\mathrm{SNR}(\omega)}{\int \mathrm{SNR}(\omega) d\omega} \mathcal{A}(\theta_0,\theta)^{(c)}_{S_0} - \frac{1}{\int \mathrm{SNR}(\omega) d\omega} \ln \frac{1+\mathrm{SNR}(\omega)\mathcal{A}(\theta_0,\theta)^{(c)}_{S_0}}{1+\mathrm{SNR}(\omega)} d\omega \quad (1)$$

where $\mathrm{SNR}(\omega)$ is the ratio of *received* signal to noise power,

$$\mathrm{SNR}(\omega) \triangleq \frac{\mathcal{S}_0(\omega) \|h_{\theta_0}(\omega)\|^2}{\sigma^2(\omega)}, \quad (2)$$

and $\mathcal{A}(\theta_0,\theta)^{(c)}_{S_0}$ is the analogue of the classical ambiguity function, i.e., the square of the cosine of the angle between the resultant vectors for the two values of source location.

$$\mathcal{A}(\theta_0,\theta)^{(c)}_{S_0} \triangleq \frac{|h_{\theta_0}(\omega)^H h_\theta(\omega)|^2}{\|h_\theta(\omega)\|^2 \|h_{\theta_0}(\omega)\|^2}.$$

Note that this function can be written using the orthogonal projection operator onto the (one-dimensional) space spanned by the vector $h_\theta(\omega)$:

$$\mathcal{A}(\theta_0,\theta)^{(c)}_{S_0} = \frac{\left\|\Pi_{h_\theta(\omega)}[h_{\theta_0}(\omega)]\right\|^2}{\|h_{\theta_0}(\omega)\|^2}$$

B. Spatial Modeling

When the *spatial model* is used, $b(\theta)$ is modeled as an unknown deterministic vector, $b(\omega)$, and the spectral density of the observations has the following form:

$$\mathcal{R}_\theta(\omega) = \sigma^2(\omega) I + \mathcal{S}(\omega) D(\theta) b(\omega) b(\omega)^H D(\theta)^H$$

Simultaneous lack of knowledge of $\mathcal{S}(\omega)$ and $b(\omega)$ implies that only the product $\sqrt{\mathcal{S}(\omega)} b(\omega)$ can be determined, i.e., the only restriction on the noiseless component of $\mathcal{R}_\theta(\omega)$ is that it has rank one, meaning that all the replicas are perfectly correlated. This increased uncertainty leads to [5] the following expression for the ambiguity

$$\mathcal{A}(\theta_0,\theta)^{sp}_{b_0} = \int \frac{\mathrm{SNR}(\omega)}{\int \mathrm{SNR}(\omega) d\omega} \left[\mathcal{A}(\theta_0,\theta)^{(d)}_{b_0} - \frac{1}{\mathrm{SNR}(\omega)} \ln \frac{1+\mathrm{SNR}(\omega)\mathcal{A}(\theta_0,\theta)^{(d)}_{b_0}}{1+\mathrm{SNR}(\omega)}\right] d\omega \quad (3)$$

where $\mathrm{SNR}(\omega)$ is defined by eq. (2), and

$$\mathcal{A}(\theta_0,\theta)^{(d)}_{b_0} \triangleq \frac{\left\|\Pi_{\mathcal{H}(\theta)} D(\theta_0) b_0\right\|^2}{\|D(\theta_0) b_0\|^2},$$

and $\Pi_{\mathcal{H}(\theta)}$ denotes the orthogonal projection operator into the subspace $\mathcal{H}(\theta)$, generated by the P steering vectors

(columns of the matrix $D(\theta)$) that correspond to the scanning location θ.

Note that in this case the one dimensional vector $h_\theta(\omega)$ is replaced by the P-dimensional subspace spanned by the individual steering vectors. This fact is an immediate consequence of having a larger number of degrees of freedom on the model that is being fitted to the observations.

3. Overall Structure

In this section we show plots of the ambiguity surface for the complete propagation model (see section 2.A), over a region extending from the near zone to the second convergence zone. We consider a deep ocean area (bottom depth is 5 Km), with a bilinear velocity profile with the duct axis located 914 meters below surface, and a negative velociy gradient of $-.035sec^{-1}$ in the upper layer, and of $.013sec^{-1}$ between the duct and the bottom. A smooth sea surface and a medium-silt bottom type were considered. The wind speed is 3 knots. The maximum number of bottom reflections is limited to two.

For all cases, the array is linear, vertical, with 5 sensors spaced 6 meters apart, the first sensor being located at a depth of 240 meters. The signal emitted by the source has a spectrum flat up to 1 KHz.

The next figure shows density plots for three different source positions: in the near zone (a), in the first shadow zone (b) and in the first convergence zone (c). The limits of the grid of analysis are indicated in the plots. Darker values corespond to small ambiguity values, and clear zones to high ambiguity. The true source location is indicated by a white dot. The vertical structure of the ambiguity surfaces, corresponding to the alternation between shadow and convergence zones is clearly displayed. We see that sources in the shadow zones lead to simpler ambiguity surfaces, mostly confined to the true shadow zone, with secondary lobes of small amplitude in the other shadow zones. The ambiguity structure produced by sources in the convergence zones is more complex, due to the richer ray structure, that includes, in general, all kinds of rays (bottom and surface reflected and purely refracted). The ambiguity surface tends to get more difuse (smeared) with increased distance from the antenna, i.e., its more spread out for sources in the second convergence zone than for sources in the first convergence zone. The secondary lobes of ambiguity are formed predominantly in the other convergence zones as well as in the near zone. Lack of space precludes the inclusion of other configurations here, which would illustrate the behaviour of ambigutiy with respect to the antenna's depth and source signal bandwidth. We can state, however, that the observability conditions depend very strongly on the antenna's location. Increasing

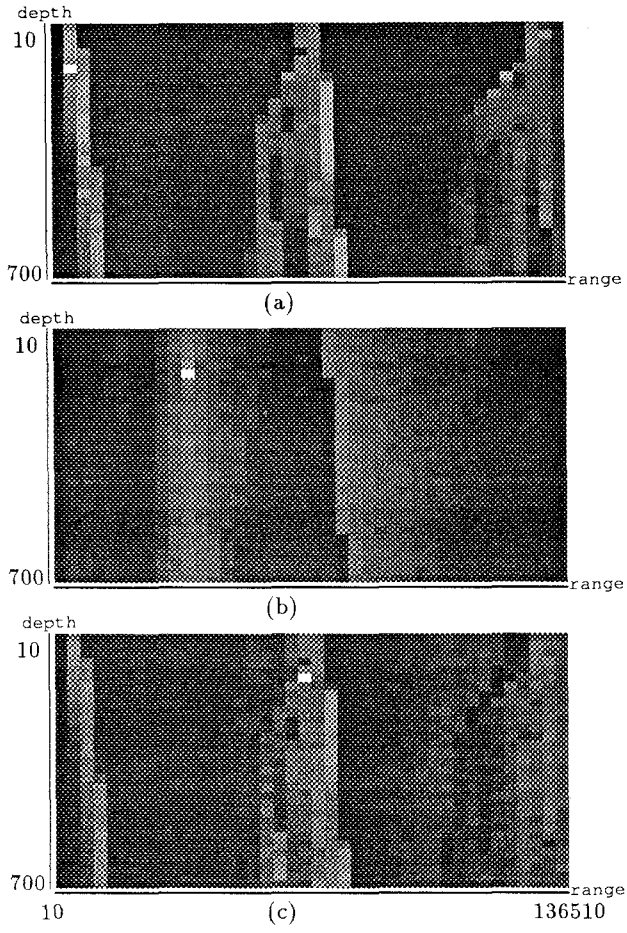

Figure 1: Ambiguity surfaces: deep ocean areas.

the signal's bandwidth always leads to better source location identifyability.

We point out that the temporal structure of the observed wavefield is determinant in resolving ambiguity in these plots, since, over most of the signal bandwidth, we have a sensor spacing larger than the Nyquist spatial frequency.

4. Near Zone

In this section we discuss the ambiguity structure of the Near Zone. In this zone there is a direct ray between the source and the receiving sensors, i.e., a ray that has neither suffered a boundary reflection nor has crossed the duct's axis. This is the zone where the simple straight path propagation can yield approximate results. Note that the extension of this zone depends both on the antenna depth (increasing with proximity of the antenna to the duct), and of the velocity gradients (that determine the ray's curvature). All the examples shown above consider

the same velocity profile as in the previous section, and the grid of analysis is indicated in the plots. The source is located at a range of 3.5 Km and a depth of 130 meters.

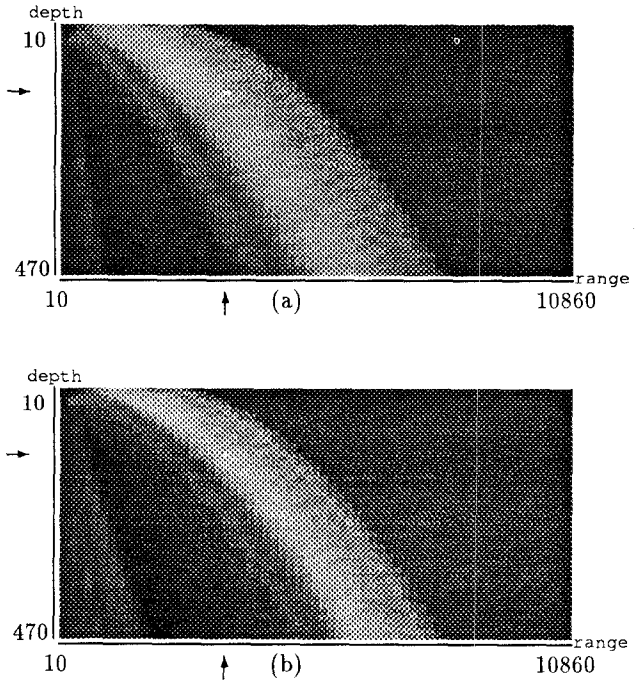

Figure 2: Near Zone, antenna at 20 meters.

Fig. 2 considers an antenna at a depth of 20 meters, showing the ambiguity surfaces for sources with bandwidths of $500Hz$ (a) and $1KHz$ (b). As expected, the lobes of the ambiguity function are narrower for the larger bandwidth, which is due to the increased delay resolving power with increased frequency. Note that the curvature of the rays is noticeable, as well as the boundary bewteen the near zone and the first shadow zone. In this zone, the ambiguity has an almost radial structure, with greater values in the region corresponding to a cone of angle of arrivals in the neighborhood of the direct ray.

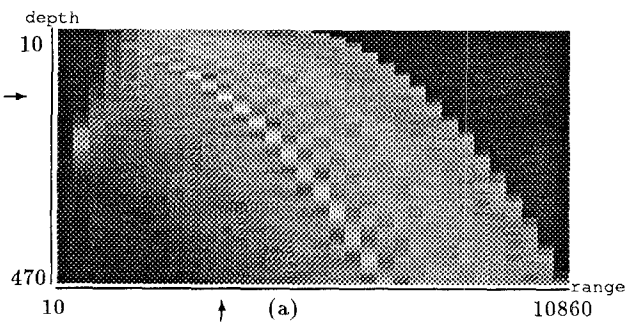

In Fig. 3 we plot the ambiguity surface when the antenna is located closer to the duct's axis, 240 meters deep.

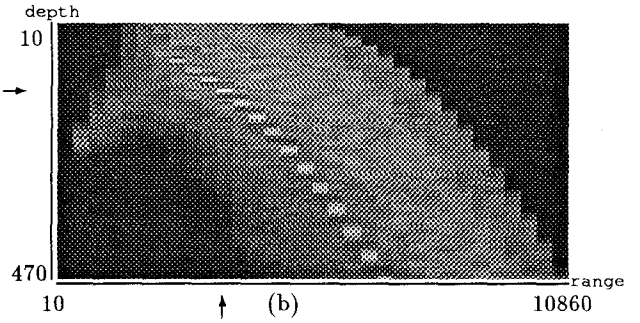

Figure 3: Near Zone, antenna at 240 meters.

We see that although a broader mainlobe exists, its shape is considerably different from the previous case, with a marked peak structure. This is expecially true when comparing the surfaces obtained for the larger bandwidth of 1 KHz (i.e., Figs. 2(b) and 3(b)). Note also that the small secondary lobe in Fig. 2 corresponding to paths incoming from the bottom is not present in Fig. 3, but that there is some ambiguity with source locations located radially between the source and the antenna.

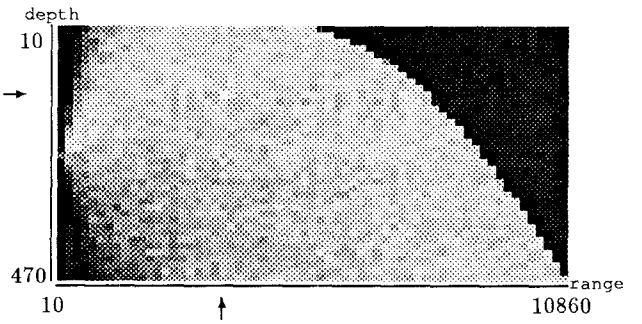

Figure 4: Near Zone, 5 sensors at 20 meters, spatial model.

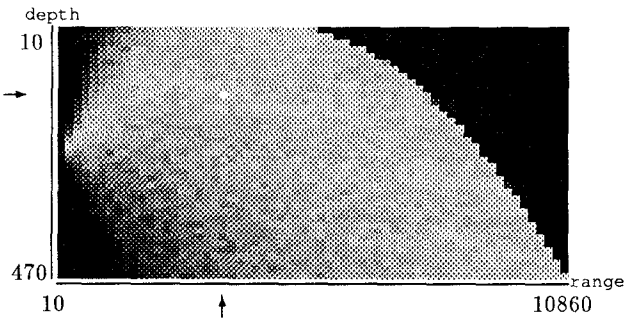

Figure 5: Near Zone, 10 sensors at 20 meters, spatial model.

To assess the importance of modeling also the temporal delays, besides the spatial structure of the received wavefield, we show in Fig. 4 the density plot of the ambiguity

surface for a source with a narrowband spectrum around 1 Khz. A 5 element vertical antenna is located at a depth of 240 meters, with inter-sensor spacing of $d = .6$ meters. From this plot we conclude that there is a wide ambiguous region, corresponding to source locations inside a curved cone with vertex at the antenna. The detailed sidelobe structure is not visible in this plot due to the granularity of the grid. Comparison of this plot with the previously presented surfaces demonstrates the clear superiority of the complete modeling approach. Fig. 5 shows the ambiguity surface for an array with 10 sensors. Comparison with Fig. 4 reveals a slight improvement on observability.

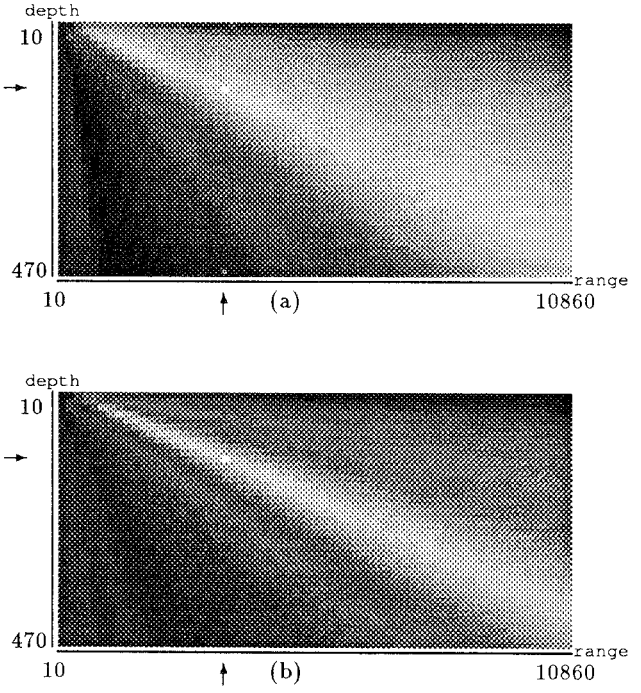

Figure 6: Near Zone, antenna at 20 meters, isovelocity model.

Fig. 6 displays the ambiguity surface obtained with an isovelocity model, considering only a direct ray and two reflected rays, one reflected at the surface and the other at the bottom. The antenna is located at 20 meters. Note the similarity between Figs. 2 and 6. Naturally, this simple model is not able to predict the existence of the shadow zone, which justifies the distinct behaviour of the two plots at larger distances.

5. Shadow Zone

This region is characterized by the existence only of rays that have relected at least on one of the medium's boundaries (either the surface or the bottom). It corresponds to arrival angles near to the end-fire direction (for a vertical array), as well as to lower levels of received energy. The bilinear velocity profile and the array are as described in section 3. Two values of array depth are shown: 20 and 240 meters. The density plots are done over interval $20010m \leq R \leq 30860m, 10m \leq y \leq 470m$.

The source is located at a horizontal distance $R = 23510$ meters, and at a depth of $y = 130$ meters.

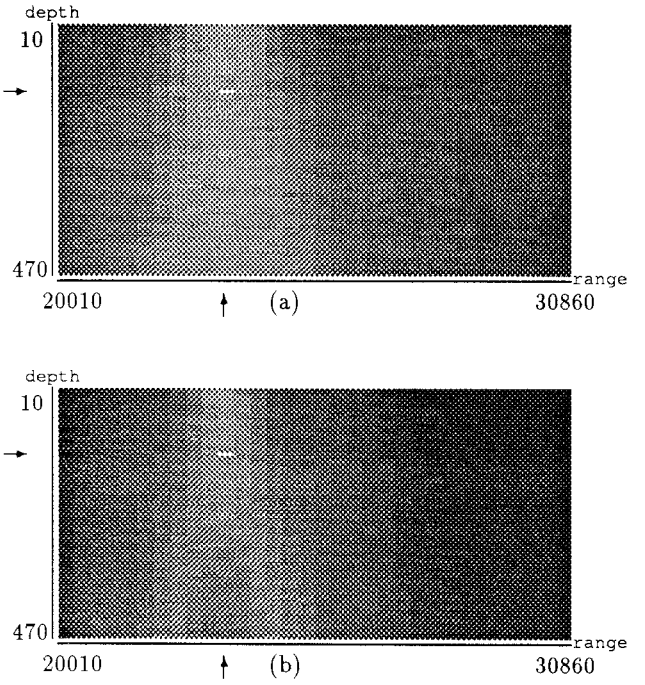

Figure 7: Shadow Zone, antenna at 20 meters.

In this zone, we observe a very good ambiguity structure, with a sharp peak at the true source location and no apreciable side lobes. This behaviour is explained by the fact that the inter-path delays have large values, and are thus well resolved at the frequencies of analysis.

6. First Convergence Zone

This section presents the ambiguity structure of the first convergence zone, i.e., where purely refracted rays, having at least crossed once the duct axis arrive from the source at the receiving antenna. As for the two previous cases, the location of this zone depends heavily on the velocity profile considered and on the antenna's depth. For the cases under consideration here, i.e., the bilinear velocity profile presented in section 3, and antennas depths up to 240 meters, distances on the range $63010m \leq R \leq 73860m$ and depths $10m \leq y \leq 460m$ were considered for ploting the ambiguity surface. In this zone, the ray curvature can no longer be ignored, the propagation structure predicted

by naive isovelocity profiles being completely wrong. In the plots, the source is located at a range of 66.5 Km and 130 m below surface.

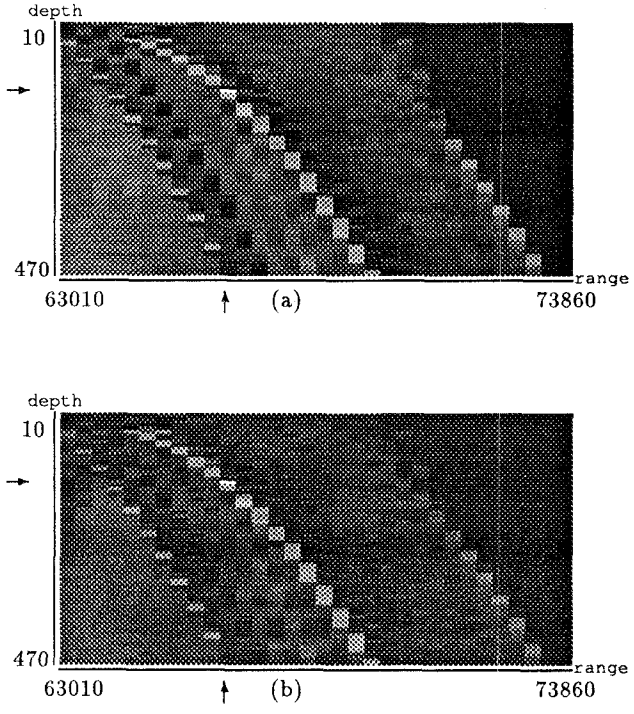

Figure 8: Convergence Zone, antenna at 20 meters.

Comparing the plots for the two antenna's depths, we see that a clear improvement is noticeable when the source is deeper in the water column. This fact is also visible in the plots of the Near Zone, although its effect is more marked here. The fine structure of the surfaces is directly related to the propagation strcture, and all the artifacts of the bilinear approximation to the velocity profile are clearly displayed in the curves presented.

7. Conclusions

We presented plots of ambiguity surfaces for source localization, assuming for very general cenarios, which demonstrate its validity as a tool for global performance analysis. In general, we see that the ambiguity surfaces have a complex form, strongly dependent on the particular propagation and observation conditions. In general, these surfaces possess secondary lobes of non-negligible amplitude, proving that an error analysis based solely on its local curvature (i.e., Cramer-Rao bounds) may give very optimistic estimations of the actual error levels.

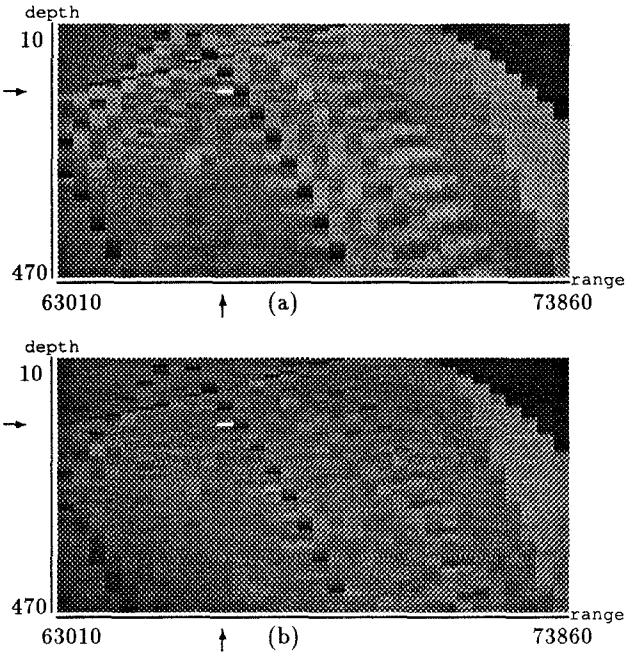

Figure 9: Convergence Zone, antenna at 240 meters.

Acknowledgments

The authors would like to acknowledge the assistance of Maria Paula Santana in the development of the software package that produced the plots included in this paper.

References

[1] J. M. F. Moura and M. J. D. Rendas. Optimal filtering in the presence of multipath. In C. R. Baker, editor, *Stochastic Processes in Underwater Acoustics, Lecture Notes in Control and Information Sciences # 85*. Springer-Verlag, N.Y., 1986.

[2] M. João D. Rendas and José M. F. Moura. Ambiguity analysis in source localization with unknown signals. In *Int. Conf. on Acoustic, Speech and Signal Processing91, Toronto, Canada*, May 1991.

[3] M. João D. Rendas and José M. F. Moura. Cramer-Rao bounds for source location systems in multipath environments. *IEEE Trans. on Acoustic, Speech and Signal Processing*, Vol. 39, No. 12:2593–2610, Dec. 1991.

[4] M. João D. Rendas and José M. F. Moura. Ambiguity analysis in source location. *Submitted for publication*, May, 1991.

[5] Maria João Rendas. *Erro e Ambiguidade em Sistemas de Localização*. PhD thesis, Instituto Superior Técnico, Lisboa, 1991.

[6] P. M. Woodward. *Probability and Information Theory, with Applications to RADAR*. Pergamon Press, 1953.